






Article

Chemical Composition and Deposition Characteristics of Precipitation into a Typical Temperate Forest in Northeastern China

Yingying Wang^{1,2}, Feifei Zhu^{1,3,4} , Ronghua Kang^{1,4,5}, Linlin Song^{1,3,4}, Shaonan Huang⁶, Dan Huang^{1,4}, Kai Huang^{1,2} , Abubakari Said Mgelwa^{1,7} , Geshere Abdisa Gurmessa^{1,4} , Xiaoming Fang^{1,3,4} and Yunting Fang^{1,4,*} 

- ¹ CAS Key Laboratory of Forest Ecology and Management, Institute of Applied Ecology, Chinese Academy of Sciences, Shenyang 110016, China
 - ² University of Chinese Academy of Sciences, Beijing 100049, China
 - ³ Qingyuan Forest CERN, National Observation and Research Station, Shenyang 110016, China
 - ⁴ Key Laboratory of Stable Isotope Techniques and Applications, Shenyang 110016, China
 - ⁵ Weifang Academy of Modern Agriculture and Ecological Environment, Weifang 261000, China
 - ⁶ Key Laboratory of Geospatial Technology for the Middle and Lower Yellow River Regions, Ministry of Education, College of Geography and Environment Science, Henan University, Kaifeng 475004, China
 - ⁷ College of Natural Resources Management & Tourism, Mwalimu Julius K. Nyerere University of Agriculture & Technology, Musoma P.O. Box 976, Tanzania
- * Correspondence: fangyt@iae.ac.cn



Citation: Wang, Y.; Zhu, F.; Kang, R.; Song, L.; Huang, S.; Huang, D.; Huang, K.; Mgelwa, A.S.; Gurmessa, G.A.; Fang, X.; et al. Chemical Composition and Deposition Characteristics of Precipitation into a Typical Temperate Forest in Northeastern China. *Forests* **2022**, *13*, 2024. <https://doi.org/10.3390/f13122024>

Academic Editor: Roger Seco

Received: 17 October 2022

Accepted: 27 November 2022

Published: 29 November 2022

Publisher's Note: MDPI stays neutral with regard to jurisdictional claims in published maps and institutional affiliations.



Copyright: © 2022 by the authors. Licensee MDPI, Basel, Switzerland. This article is an open access article distributed under the terms and conditions of the Creative Commons Attribution (CC BY) license (<https://creativecommons.org/licenses/by/4.0/>).

Abstract: The chemical compositions and deposition characteristics of atmospheric precipitation affect the structure and function of forest ecosystems and reflect regional air quality. Although northeastern China constitutes a vital forested area, few relevant studies reveal the chemical composition and the nitrogen (N) and sulphur (S) deposition characteristics within precipitation. In this study, we monitor precipitation chemistry during 2018–2020 at a rural forested site in northeastern China (the Qingyuan site) and compare it with those from background sites (Mondy in Russia and Ochiishi in Japan) and highly anthropogenically influenced areas (Beijing). The precipitation pH range was 4.7–8.0 (volume-weighted average 6.2). The average concentration of total ions in precipitation was 459 $\mu\text{mol L}^{-1}$, representing a moderate pollution level. Nitrate (NO_3^- , 73 $\mu\text{mol L}^{-1}$) and ammonium (NH_4^+ , 133 $\mu\text{mol L}^{-1}$) were the major anions and cations in the precipitation. Total inorganic nitrogen (TIN) deposition was 12.3–15.9 $\text{kg N ha}^{-1} \text{ year}^{-1}$ (NH_4^+ -N deposition accounted for 54–67%), lower than the average level in China (19.4 $\text{kg N ha}^{-1} \text{ year}^{-1}$). Annual precipitation sulphate (SO_4^{2-}) deposition was 4.9–6.7 $\text{kg S ha}^{-1} \text{ year}^{-1}$. Seventy-two percent of the precipitation ions at our site originated from human activities. This work has revealed that N and S deposition is an important ion deposition component in atmospheric precipitation in the study of temperate forests in northeastern China. Nitrogen deposition, as a source of vital nutrients in the forest ecosystem, may promote forest growth and, thereby, forest carbon sequestration.

Keywords: chemical composition; forest; nitrogen deposition; northeastern China; precipitation; source contribution; sulphur deposition

1. Introduction

Atmospheric concentrations of nitrogen oxides (NO_x), ammonia (NH_3) and ammonium (NH_4^+) (collectively NH_x), and sulphur dioxide (SO_2), and the deposition of nitrogen (N) and sulphur (S) have rapidly increased over the past 100 years owing to increasing anthropogenic emissions, such as massive fossil fuel combustion, motor vehicle emissions, and fertiliser application [1–4]. Precipitation is a necessary removal process for atmospheric pollutants; therefore, the chemical composition of atmospheric precipitation can reflect regional atmospheric pollution status. In addition, precipitation is a water source for forest

ecosystems and a significant nutrient source, such as of N, S, Ca, and Mg [5]. Through precipitation, rain (snow) water carries airborne aerosol particles and gases, such as NO_x , NH_x , and SO_2 , into forest ecosystems [6,7]. Although elevated N deposition input can enhance plant productivity and carbon sinks in forest ecosystems, excess N loading can have many negative effects, including soil acidification, eutrophication of water bodies, loss of biodiversity, and forest decline [3,8–12]. By analysing the ion deposition level in atmospheric precipitation, it is possible to effectively infer the input of nutrients into forest ecosystems [13] and determine the extent of atmospheric pollution in the region and the pathways of material sources through changes in chemical components, pH, and other chemical characteristics [14]. Therefore, the chemical composition and deposition of precipitation in forests have been significant issues in forest hydrological and ecological research [5,9,11,15].

China is one of the regions worldwide with high nitrogen and sulphur deposition [16,17]. Atmospheric N deposition in China increased by 60% from 1980 to 2010 [18] and stabilised from 2016 to 2020 [19] because of the socioeconomic development and transformation of the energy structure. The total nitrogen deposition in northern China is $60.6 \text{ kg N ha}^{-1} \text{ year}^{-1}$ [20], which is much higher than the monitored results in North America ($5.3 \text{ kg N ha}^{-1} \text{ year}^{-1}$), East Asia ($8.7 \text{ kg N ha}^{-1} \text{ year}^{-1}$), Europe ($10.6 \text{ kg N ha}^{-1} \text{ year}^{-1}$), and other countries or regions [21–26]. An increasing number of studies have shown the current status of precipitation chemistry in urban and suburban areas of China. However, rural and forested areas in China have been paid less attention compared to urban or suburban areas, possibly because of the relatively less severe pollution, public awareness, and the attention paid to environmental issues from the big cities [27–31]. Forested areas are more sensitive to air pollution and can show a larger response to N deposition than their non-forested counterparts. Related deposition characteristics of certain ions in forested areas, i.e., nitrogen and sulphur, were even less demonstrated.

The temperate forest region in northeastern China is located in the Daxing'anling, Xiaoxing'anling, and Changbai Mountains, the largest natural forest area in China and a natural ecological barrier for the northeastern, northern China, and even northeastern Asia. With high forest cover, it represents a crucial carbon sink and plays an essential role in absorbing CO_2 and mitigating climate warming. Precipitation carrying various ions serves as a source of nutrient input into forest ecosystems. By alleviating N limitation in some forests, N deposition would lead to enhanced plant productivity and potentially forest C sink. Several studies indicated that large long-term N deposition resulted in the N saturation phenomenon in Japan and China. After that, forest decline symptoms were observed in Japan and China [32]. However, information about air pollution in China's rural forests is scarce. Few rural forest lands are subjected to ambient air quality measurements in northeastern China [33], with few studies reporting precipitation deposition of ions in forested regions therein [32–35]. We particularly lack data on the amounts and sources of atmospheric deposition into rural forests in northeastern China. Therefore, quantifying and assessing ion deposition in temperate forests in northeastern China, and comparing it with heavily polluted and clean areas, is essential.

In this study, we collected precipitation samples on a daily basis at a rural Qingyuan forest site in northeastern China from 2018 to 2020 to analyse the chemical composition of the precipitation. We compared this site with a high-deposition site in Beijing, representative of northern China, and two remote monitoring sites in East Asia (Mondy and Ochiishi) as low-deposition background sites. The objective of our research was to: (1) analyse the chemical composition characteristics of precipitation from the study forest and quantify the deposition of major ions in typical temperate forest areas in northeastern China; (2) assess the current status through comparison with other high and background sites; and (3) determine the contribution of anthropogenic sources and related transport pathways of major precipitation ions and provide a reference basis for atmospheric environmental management. We hypothesized that N and S deposition into our study forest would be

lower than those of urban areas in China and still much higher than those into very remote sites at similar latitudes.

2. Materials and Methods

2.1. Study Site and Sample Collection

Precipitation samples were collected from the Qingyuan Forest Station of the Chinese Ecosystem Research Network (Qingyuan Forest CERN), located in Qingyuan County, Liaoning Province, northeastern China (41°51' N, 124°54' E), at altitudes of 578 m. The area has a continental monsoon climate with warm and rainy summers and cold and dry winters [36]. Over the 3-year study period, the annual mean air temperature was 4.8 °C, with a minimum of −27.8 °C in January and a maximum of 27.0 °C in July. The mean annual precipitation was 743 mm, with the rainy season concentrated in summer and autumn, accounting for 70–80% of the yearly rainfall. There are no prominent pollution sources within a 50 km radius of the study area, and this region is with forest coverage of over 90% [36,37].

A total of 109 rain and 13 snow samples were collected from January 2018 to December 2020. Detailed information on the sample collection and processing procedures is available from Huang et al. (2019) [38]. The bulk deposition samples were collected on a daily basis with three manual rain gauges (20 cm in diameter). The samplers were installed at 1.5 m aboveground at the meteorological observation field (25 m × 25 m) [37–39], with no trees or high buildings nearby. After each collection, the samplers were washed with deionized water (Figure 1, Figure S1). The pH of the precipitation samples was measured immediately after collection. Precipitation samples were filtered through 0.45 µm nylon membrane filters and stored in clean 100 mL white polypropylene plastic bottles at −20 °C until chemical analysis. Snow samples were melted at room temperature, filtered, and stored according to the precipitation procedure. Three precipitation samples collected from three separate samplers during the same period were mixed as one composite sample to determine ion concentrations. The monitoring included precipitation amount, pH, NH₄⁺, Ca²⁺, K⁺, Mg²⁺, Na⁺, SO₄^{2−}, NO₃[−], Cl[−], and F[−] concentrations in precipitation.

2.2. Chemical Analyses

Chemical analyses were conducted at the Stable Isotope Laboratory of the Institute of Applied Ecology, Chinese Academy of Sciences. Concentrations of major inorganic ions in the samples were determined using an ion chromatograph (DionexTM, ICS-600, Thermo Fisher Scientific Instrument Co., LTD, USA) with an instrument accuracy of 5%. The concentrations of cations (NH₄⁺, Ca²⁺, K⁺, Mg²⁺, and Na⁺) were determined using DionexTM CS12A and CQ12A columns, with 10 mmol L^{−1} methanesulfonic acid as the eluent at a flow rate of 1.0 mL min^{−1}. The concentrations of anions (SO₄^{2−}, NO₃[−], Cl[−], and F[−]) were determined using the DionexTM AS22 and AQ22 columns. The leaching solution was 4.5 mmol L^{−1} of sodium carbonate (Na₂CO₃) plus 1.4 mmol L^{−1} sodium bicarbonate (NaHCO₃) with a flow rate of 1.2 mL min^{−1}.

2.3. Data Sources and Quality Control

The total anion and cation concentrations of the precipitation samples were determined to control their quality standards by referring to the United States Environmental Protection Agency (USEPA) [40] and the Technical Manual for Wet Deposition Monitoring in East Asia, 2010 [41]. Additional ionic imbalances may be due to unmeasured organic acids in rainwater [41], such as hydrogen carbonate (HCO₃[−]) and organic ions like formate (HCOO[−]) and acetate (CH₃COO[−]), which were not measured, and data regarding any organic acids were not available. After rejecting the data that did not meet the quality criteria, linear regression analysis was performed between the grand total of anion concentration and the grand total of cation concentration for the Qingyuan site. The regression analysis of total anion and cation concentrations was performed for all valid precipitation samples over three years, and the R² of linear regression was 0.75 with a slope of 1.16 (Figure S2).

This indicated that the correlation between the total anions and cations was high, and all samples met the requirements.

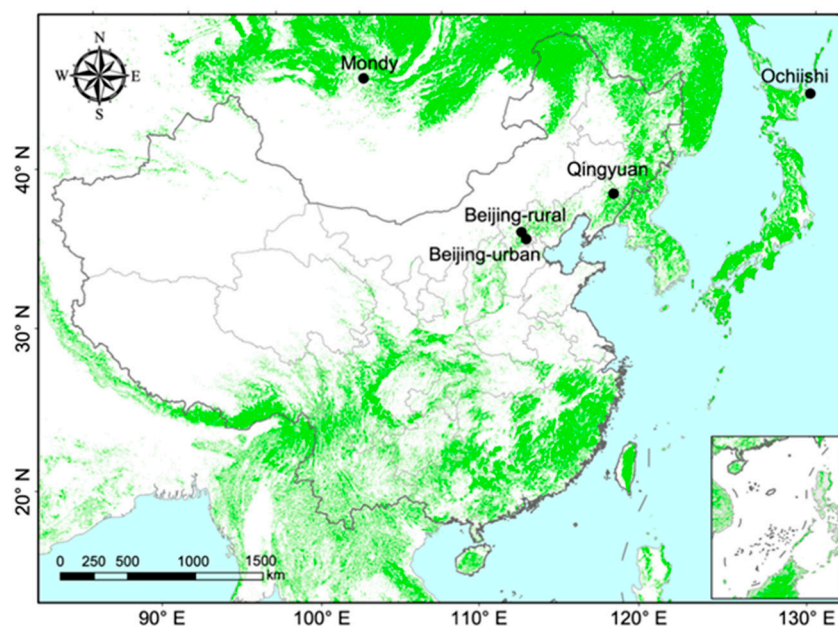


Figure 1. The locations of the Qingyuan forest study site and other sites with similar latitudes for comparison. Mondy in Russia and Ochiishi in Japan represent the clean interior and coastal sites, respectively. Beijing-urban and Beijing-rural in China represent the sites heavily influenced by urban and agricultural activities, respectively. The green areas indicate forest cover (URL: https://www.esa.int/ESA_Multimedia/Images/2018/09/2015_global_land_cover_map#.YWo7MMJQ1bU.link, accessed on 18 October 2022).

We selected two clean sites in East Asia with similar latitudes to the Qingyuan site as background sites to compare. One site was Ochiishi (43°09' N, 145°29' E) in Hokkaido City, Japan, with an elevation of 49 m, representing a clean seaward site. The other site was Mondy (51°37' N, 100°55' E) in Russia, with an elevation of 1996 m, representing a clean inland site (Figure 1). Both sites had low anthropogenic disturbances and were located more than 50 km from significant pollution sources, such as cities, power plants, and highways, and more than 500 m from major roads (less than 500 vehicles per day). Data from these two sites were obtained from the Acid Deposition Monitoring Network in East Asia during 2018–2020 (EANET) (<http://www.eanet.asia>, accessed on 20 April 2022). We further selected two other sites in urban (39°57' N, 116°19' E) [32] and rural (40°29' N, 115°59' E) [31] Beijing (Figure 1) to represent sites highly influenced by urban and agricultural activities to compare with our site (rural).

2.4. Quantitative Assessment of Ion Sources

The principal sources of ion components in rainwater include seawater sputtering, rock (soil) weathering, and anthropogenic activities (excluding the contributions of volcanoes and other natural sources [42]). To further investigate the different sources of ions in the Qingyuan precipitation, Equations (1) to (3) were used to calculate the relative contributions of the sea salt fraction (SSF), crust fraction (CF), and anthropogenic source fraction (AF):

$$SSF = (X/Na^+)_{seawater}/(X/Na^+)_{precipitation} \times 100\% \quad (1)$$

$$CF = (X/1/2Ca^{2+})_{soil}/(X/1/2Ca^{2+})_{precipitation} \times 100\% \quad (2)$$

$$AF = 100\% - SSF - CF \quad (3)$$

where X is the target ion ($\mu\text{mol L}^{-1}$), the ratio of $[X/\text{Na}^+]_{\text{seawater}}$ refers to the existing literature [43], and the $[X/\text{Ca}^{2+}]_{\text{soil}}$ is from the crustal composition (Table S1) [44]. The contributions of the crustal, oceanic, and anthropogenic sources to the ions were calculated to quantify the origins of the major ions.

2.5. Air Mass Back Trajectories

In this study, the air mass movement was set to end at the Qingyuan site using the downloaded Hybrid Single Particle Lagrangian Integrated Trajectory (HYSPLIT) version 4.0 (<http://ready.arl.noaa.gov/HYSPLITtraj.php>, accessed on 10 August 2022) [45,46]. The simulation height was 500 m (above ground level) [47], the simulation time was post-72 h, and the sampling period was within 12 h (0:00, 12:00, and 24:00 UTC). The airflow trajectory was clustered according to the velocity and direction of the horizontal airflow movement. The 3-day backward trajectories were calculated for all sampling days to track the source of water vapour in this study area for different seasons during 2020. The meteorological data used in the trajectory model were obtained from the global data assimilation system of the National Centers for Environmental Prediction (NCEP) of the United States.

2.6. Calculations and Statistical Analyses

The annual NO_3^- -N deposition in precipitation is the sum of the NO_3^- concentration multiplied by the precipitation amount for each precipitation sampling over the same year [29]. Other ion depositions were calculated in the same way as the NO_3^- -N deposition. Significance analysis was performed using the SPSS software (version 26.0; SPSS Inc., Chicago, IL, USA). One-way analysis of variance (ANOVA) was used to examine the seasonal variation of ion concentrations and deposition differences using the Duncan method. LOESS (Local Regression) was performed to fit loess-smoothed curves to determine monthly trends of ion concentration. Pearson's correlation analysis was used to determine the relationship between monthly precipitation, monthly mean ion concentration, and monthly deposition, and the analyses were performed using the R statistical software 4.1.2. Statistical significance was set at $p < 0.05$ unless otherwise stated.

3. Results

3.1. Ion Concentration and Deposition in Precipitation

During the study period, the pH of precipitation at the Qingyuan site ranged from 4.7 to 8.0 (average 6.2, Table 1). The total ion concentration of the precipitation ranged from 421 to 530 $\mu\text{mol L}^{-1}$ (average 459 $\mu\text{mol L}^{-1}$). The main cations in the precipitation were NH_4^+ and Ca^{2+} , accounting for 29% and 19% of the total precipitation ion concentration, respectively (Figure 2c). The NH_4^+ and Ca^{2+} concentrations were 97–175 (133 ± 40) $\mu\text{mol L}^{-1}$ and 74–101 (87 ± 13) $\mu\text{mol L}^{-1}$, respectively. The dominant anions were NO_3^- and SO_4^{2-} , accounting for 16% and 14% of the total ion concentration, respectively (Figure 2c). The NO_3^- and SO_4^{2-} concentrations were 58–85 (73 ± 14) $\mu\text{mol L}^{-1}$ and 56–72 (61 ± 9) $\mu\text{mol L}^{-1}$, respectively.

Over the study period, the NO_3^- -N and NH_4^+ -N deposition rates were 4.9–7.3 (5.9 ± 1.3) $\text{kg ha}^{-1} \text{ year}^{-1}$ and 6.7–19.8 (8.4 ± 1.6) $\text{kg ha}^{-1} \text{ year}^{-1}$, respectively. SO_4^{2-} -S deposition ranged from 4.9 to 6.7 (5.6 ± 0.9) $\text{kg S ha}^{-1} \text{ year}^{-1}$ (Table 1), and Ca^{2+} and Mg^{2+} depositions were 6.6–12.1 (8.9 ± 2.9) $\text{kg Ca ha}^{-1} \text{ year}^{-1}$ and 0.9–2.2 (1.7 ± 0.7) $\text{kg Mg ha}^{-1} \text{ year}^{-1}$, respectively (Table 1).

Table 1. The annual deposition of inorganic NO_3^- -N, NH_4^+ -N, total inorganic N (TIN), SO_4^{2-} -S, Ca^{2+} , and Mg^{2+} and the volume-weighted mean pH in precipitation in the Qingyuan forest, compared with another four representative sites with comparable latitudes.

Areas	Altitude m	Period	pH	NO_3^- -N	NH_4^+ -N	TIN	SO_4^{2-} -S	Ca^{2+}	Mg^{2+}	References
				kg N ha ⁻¹ year ⁻¹	kg N ha ⁻¹ year ⁻¹	kg N ha ⁻¹ year ⁻¹	kg S ha ⁻¹ year ⁻¹	kg Ca ha ⁻¹ year ⁻¹	kg Mg ha ⁻¹ year ⁻¹	
Beijing-U (Urban)	20–60	2018–2020	6.4	7.3	15.4	22.7	14.7	20.9	2.6	Sun et al. (2021) [32]
Beijing-R (Rural)	500	2017–2018	6.7	4.5	11.9	16.4	6.0	31.7	4.5	Wen et al. (2020) [31]
Qingyuan (Rural)	578	2018–2020	6.2	5.9	8.4	14.3	5.6	8.9	1.7	Present study
Ochiishi, Japan (Remote)	49	2018–2020	5.1	1.0	1.0	2.0	2.8	1.2	2.0	EANET (2020)
Mondy, Russia (Remote)	1996	2018–2020	5.3	0.2	0.2	0.4	0.3	0.4	0.1	EANET (2020)

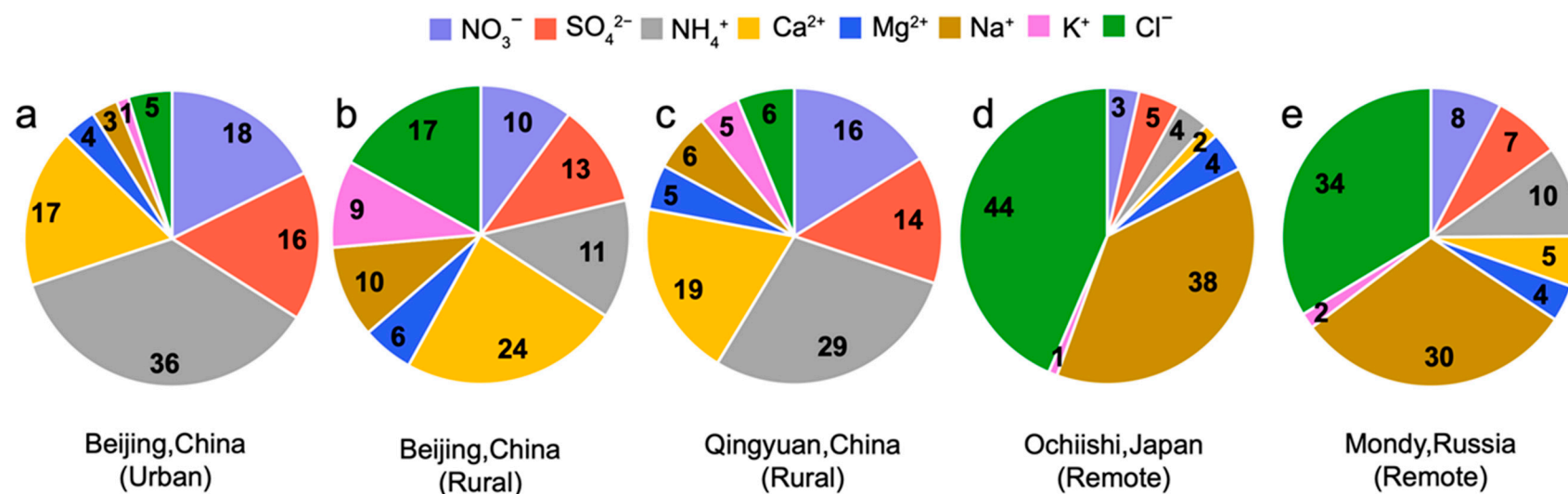


Figure 2. Percentages (%) of each ion to total ions in precipitation in Beijing urban site (a), Beijing rural site (b), the Qingyuan forest (c), Ochiishi (d), and Mondy (e) for comparison.

3.2. Seasonal Variations and Controlling Factors of Ion Concentration and Deposition

The average annual precipitation over the three-year study period was 680 mm. Precipitation was concentrated in summer (June to August) and autumn (September to November), accounting for 71% of the total annual precipitation. Seasonal trends in ion concentrations were observed, being markedly higher in spring (March to May) and winter (December to February) than in summer and autumn (Figure 3, Table 2). The average NO_3^- concentrations were 125 ± 40 , 68 ± 37 , 61 ± 20 , and $111 \pm 66 \mu\text{mol L}^{-1}$ in spring, summer, autumn, and winter, respectively (Figure 3b, Table 2). While the corresponding average NH_4^+ concentrations were 123 ± 96 , 120 ± 57 , 79 ± 70 , and $206 \pm 127 \mu\text{mol L}^{-1}$, respectively (Figure 3c, Table 2). The SO_4^{2-} concentrations averaged 181 ± 95 , 61 ± 40 , 74 ± 27 , and $148 \pm 102 \mu\text{mol L}^{-1}$ in the spring, summer, autumn, and winter, respectively (Figure 3b, Table 2). The seasonal variation in Ca^{2+} and Mg^{2+} concentrations were similar. In contrast, the seasonal characteristics of ion deposition were higher in spring and summer and lower in autumn and winter. Nitrate nitrogen deposition averaged 14 ± 7 , 13 ± 7 , 7 ± 1 , and $3 \pm 4 \text{ mol ha}^{-1} \text{ month}^{-1}$ in spring, summer, autumn, and winter, respectively, while NH_4^+ -N deposition averaged 105 ± 59 , 67 ± 23 , 36 ± 30 , and $21 \pm 20 \text{ mol ha}^{-1} \text{ month}^{-1}$ (Table 2). The precipitation of SO_4^{2-} -S deposition was 41 ± 25 , 25 ± 12 , 16 ± 6 , and $5 \pm 4 \text{ mol ha}^{-1} \text{ month}^{-1}$ in spring, summer, autumn, and winter (Table 2). The seasonal trends of Ca^{2+} and Mg^{2+} depositions were also similar.

We observed a seasonal pattern of significantly higher ion deposition in spring and summer than in autumn and winter. In addition, nitrate deposition was significantly and positively correlated with precipitation amount and concentration ($r = 0.43$, $p < 0.05$; Figure 4a,c), indicating that NO_3^- deposition was related to the amount of precipitation and atmospheric NO_3^- concentration. Except for NO_3^- , other ion depositions (including NH_4^+ , SO_4^{2-} , Ca^{2+} , and Mg^{2+}) in precipitation showed a significant positive correlation with concentration (Figure 4c,d) and no significant correlation with precipitation amount (Figure 4a,b), indicating that the ion concentration is the main factor affecting the magnitude of deposition.

3.3. Sources of Ions in Precipitation

The source contribution calculation results are shown in Figure 5. Anthropogenic input contributed the most to NH_4^+ , NO_3^- , SO_4^{2-} , and K^+ in precipitation, with contributions all above 90% (100%, 100%, 90%, and 96%, respectively; Figure 5). Generally, K^+ is mainly a land-phase input owing to the weathering of potassium feldspar and potassium-containing minerals that are eventually stored in precipitation. For K^+ in this study, the contribution of anthropogenic activities was as high as 96%, possibly owing to various anthropogenic activities, such as road dust, construction of buildings, biomass burning, and the use of potassium fertiliser. Land-phase input contributed the most to Ca^{2+} and Mg^{2+} in precipitation, accounting for 97% and 41%, respectively. These are characteristic ions that respond to terrestrial sources. The marine-phase input contributed the most to Cl^- in precipitation (84%), indicating that Cl^- is mainly a sea-saline ion. Simultaneously, the Cl^- in precipitation was influenced by anthropogenic activities (16%). Human sources of Cl^- in precipitation may include industrial emissions and coal-combustion heating in the winter of the study regions. As a whole, atmospheric precipitation ions were mainly derived from anthropogenic activities (72%) at the Qingyuan site, followed by land-phase (19%) and marine (9%) sources, indicating that the atmospheric ecology of the site is influenced mainly by anthropogenic activities (Figure S3).

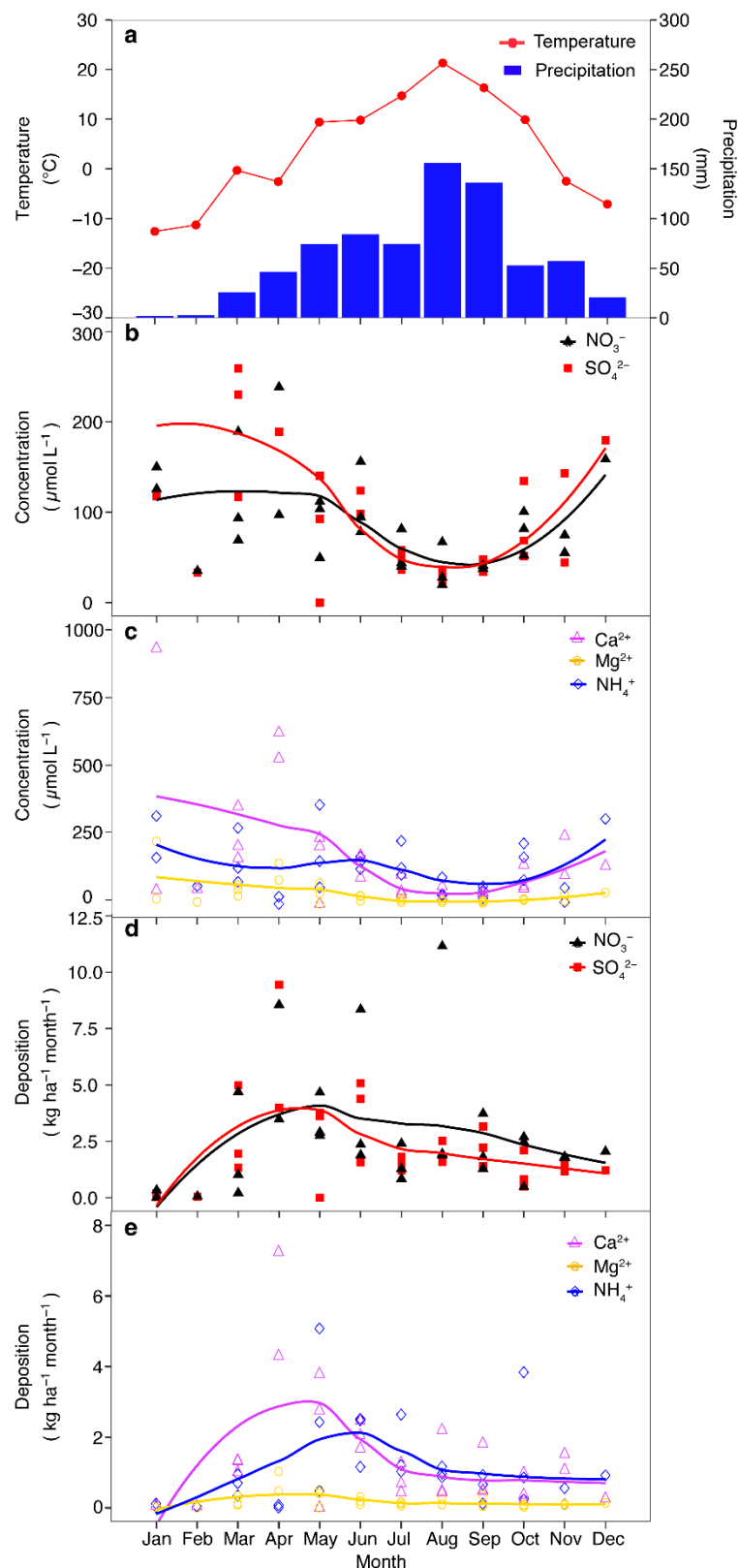


Figure 3. Monthly mean temperature and monthly mean precipitation amount (a), monthly mean concentrations (b,c), and monthly deposition rates (d,e) of major ions in precipitations in the Qingyuan forest over the period of 2018–2020. Each line in figures (b–e) indicates the loess-smoothed curve to show the monthly trends of the variables shown by the corresponding colour. The calcium ion concentration values in February 2018, January 2019, and February 2019 are missing because of the lack of enough samples for analysis.

Table 2. Seasonal mean concentrations and deposition of major ions in precipitation at the study site. Numerical means \pm SD were given. Superscript letters indicate significant differences among seasons ($p < 0.05$, one-way ANOVA, Duncan test).

Season	Concentration ($\mu\text{mol L}^{-1}$)							
	NO_3^-	NH_4^+	SO_4^{2-}	Ca^{2+}	Mg^{2+}	Na^+	K^+	Cl^-
Spring	125 \pm 40 ^a	123 \pm 96 ^{ab}	181 \pm 95 ^a	324 \pm 225	68 \pm 43 ^a	75 \pm 55	50 \pm 35 ^a	57 \pm 38 ^{ab}
Summer	68 \pm 37 ^b	120 \pm 57 ^{ab}	61 \pm 40 ^b	82 \pm 57	15 \pm 7 ^b	14 \pm 5	20 \pm 9 ^b	20 \pm 7 ^b
Autumn	61 \pm 20 ^b	79 \pm 70 ^b	74 \pm 27 ^b	99 \pm 72	15 \pm 7 ^b	58 \pm 46	14 \pm 4 ^b	29 \pm 16 ^b
Winter	111 \pm 66 ^a	206 \pm 127 ^a	148 \pm 102 ^a	314 \pm 177	82 \pm 41 ^a	55 \pm 45	22 \pm 21 ^b	72 \pm 60 ^a
Season	Deposition ($\text{mol ha}^{-1} \text{ month}^{-1}$)							
	NO_3^-	NH_4^+	SO_4^{2-}	Ca^{2+}	Mg^{2+}	Na^+	K^+	Cl^-
Spring	14 \pm 7	105 \pm 59	41 \pm 25 ^a	76 \pm 60 ^a	17 \pm 12 ^a	31 \pm 22	34 \pm 21 ^a	27 \pm 22 ^a
Summer	13 \pm 7	67 \pm 23	25 \pm 12 ^{ab}	32 \pm 17 ^{ab}	6 \pm 2 ^b	13 \pm 6	17 \pm 8 ^{ab}	19 \pm 10 ^{ab}
Autumn	7 \pm 1	36 \pm 30	16 \pm 6 ^{ab}	23 \pm 10 ^{ab}	4 \pm 2 ^b	24 \pm 22	8 \pm 6 ^{ab}	13 \pm 9 ^{ab}
Winter	3 \pm 4	21 \pm 20	5 \pm 4 ^b	4 \pm 3 ^c	3 \pm 3 ^b	5 \pm 0.3	1 \pm 0.1 ^c	6 \pm 0.4 ^c

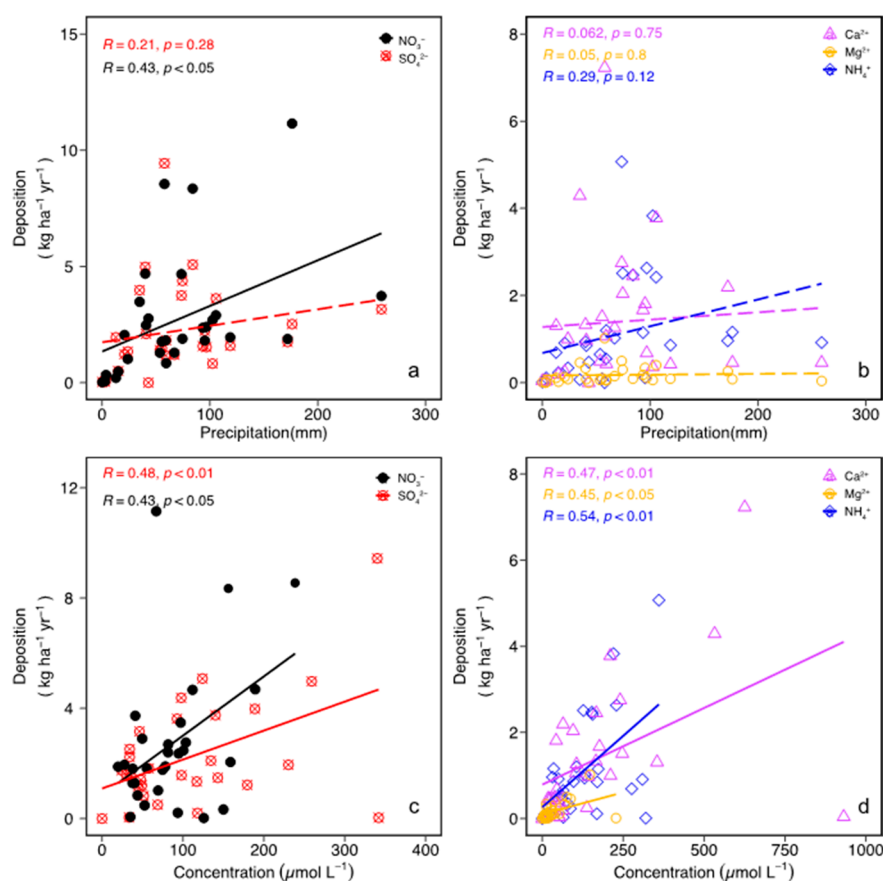


Figure 4. Correlations of monthly deposition of major ions with monthly precipitation amounts (a,b) and their concentrations (c,d) in Qingyuan throughout 2018–2020. Solid lines and dashed lines represent significant and non-significant relations, respectively.

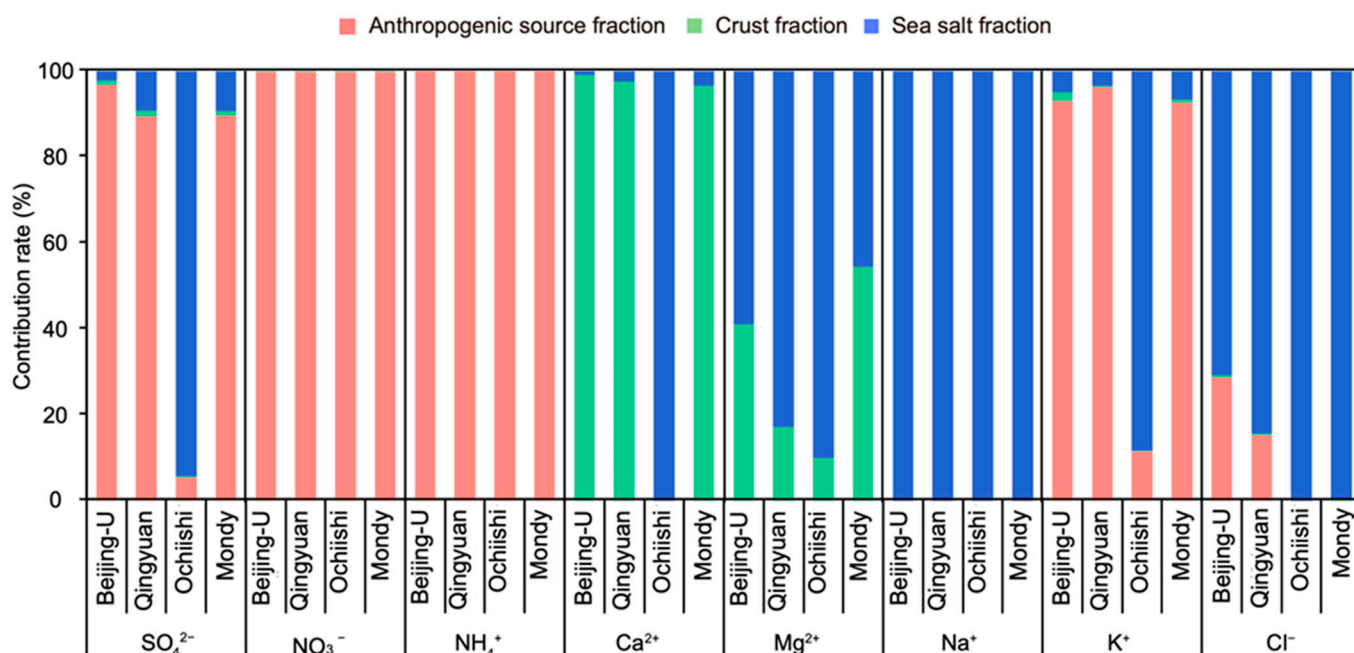


Figure 5. Contribution of each source to the major ions in precipitation into the Qingyuan forest throughout 2018–2020, compared to other representative sites at comparable latitudes.

The HYSPLIT 4.0 shows that the atmospheric precipitation water vapour sources at the Qingyuan site had significant seasonal variations during the study period. The source of ions in precipitation was influenced by water vapour transported from distant areas (24–44%), in addition to the local circulating water vapour clouds (Figure S4). Spring and summer water vapours are influenced by the East Asian monsoon, with sources mainly from the western Pacific (27–31%; Figure S4a,b). Autumn and winter water vapour were primarily derived from westerly transport with the influence of polar air masses in the Mongolian direction (32–44%; Figure S4c,d). Water vapour transport from the persistent southeast and northwest air currents at low altitudes, which also carries acidic pollutants, affects the air quality at the Qingyuan site, thus changing the precipitation chemistry characteristics in this study area, further confirming our observations.

4. Discussion

4.1. Comparisons with Urban and Background Regions

Precipitation is an effective scavenging pathway for removing gases and aerosol pollutants from the atmosphere [6,9,48]. Therefore, the chemical composition of precipitation reflects the level of atmospheric pollution. To better evaluate the current atmospheric pollution level at the Qingyuan site, this study site was compared with the Beijing urban (2018–2020) and rural (2017–2018) sites and the two background sites of Ochiishi and Mondy (2018–2020). The calculation results of the source contributions showed that the precipitation ion concentration at the Qingyuan site was most influenced by anthropogenic sources (72%). In comparison, the land-phase and marine sources accounted for 19% and 9%, respectively. The contribution of each source in Qingyuan was similar to that in Beijing (Figure S3). However, the contribution of anthropogenic sources to precipitation ions at the Qingyuan site was higher than that at the clean inland Mondy site (41%) and approximately three times that at the clean coastal Ochiishi site (26%). These results suggest that the rapid development of the regional economy and urbanisation have influenced the chemical composition of precipitation at the Qingyuan site.

We further assessed the type and level of precipitation pollutants at the Qingyuan site based on the total ion concentration. The annual mean total ion concentration of precipitation during the study period was 459 $\mu\text{mol L}^{-1}$. For total ion concentration of precipitation, our site was 25% lower than the Beijing urban site (average 575 $\mu\text{mol L}^{-1}$).

but two times higher than the coastal background site Ochiishi (average $230 \mu\text{mol L}^{-1}$) and 15 times higher than the clean inland background site Mondy (average $29 \mu\text{mol L}^{-1}$; Figure 2). Comparing annual ion deposition of precipitation (including NO_3^- -N, NH_4^+ -N, SO_4^{2-} -S, Ca^{2+} , Mg^{2+} , Cl^- , Na^+ , and K^+), the $44 \text{ kg ha}^{-1} \text{ year}^{-1}$ in the Qingyuan site amounted 64% of that in Beijing urban site ($68 \text{ kg ha}^{-1} \text{ year}^{-1}$), 80% of that in Ochiishi ($55 \text{ kg ha}^{-1} \text{ year}^{-1}$, mainly contributed by Cl^- and Na^+), and about 30 times that in Mondy ($1.5 \text{ kg ha}^{-1} \text{ year}^{-1}$; Table 1). This indicates that the northeast temperate forest region has cleaner precipitation than the urban region. However, it still experiences moderate to high pollution compared to the Mondy and Ochiishi regions.

The chemical composition of the precipitation at our study site was also markedly different from those at the other sites. The inorganic ions of atmospheric precipitation at the Qingyuan site consisted mainly of NH_4^+ , Ca^{2+} , NO_3^- , and SO_4^{2-} . The sum of their molar concentrations accounted for 78% of the total ion concentrations in precipitation (Figure 2c), similar to the values reported for many urban areas, such as Beijing (89%), Shanghai (81%), Kathmandu (88%) in Nepal, and Klang Valley (86%) in Malaysia [29,49–52]. However, the molar concentration at Qingyuan was 9% lower than that in the urban area of Beijing (87%). It was 20% higher than that in the rural area of Beijing (58%), and 5.6 and 2.6 times higher than those in Ochiishi (14%) and Mondy (30%), respectively. The clean ion of Cl^- and Na^+ concentrations in the Qingyuan site accounted for 12% of the total ion concentration in precipitation (Figure 2c), which was much lower than the two background sites, Ochiishi (82%; Figure 2d) and Mondy (64%; Figure 2e), and other coastal cities, such as Satkhira (41%) in Bangladesh and Falta (55%) in India [51].

NH_4^+ -N and NO_3^- -N deposition at our study site accounted for the largest proportion of the total ion deposition (24–44%). The average annual inorganic nitrogen deposition (TIN, NO_3^- -N plus NH_4^+ -N) at this study site was $14.3 \text{ kg N ha}^{-1} \text{ year}^{-1}$ (Table 1), which is 29% lower than the Chinese average ($19.4 \pm 0.8 \text{ kg N ha}^{-1} \text{ year}^{-1}$, based on monitoring from 2011 to 2018) [53], 35% lower than the Beijing urban area ($22 \text{ kg N ha}^{-1} \text{ year}^{-1}$), and 13% lower than the Beijing rural area ($16.4 \text{ kg N ha}^{-1} \text{ year}^{-1}$). However, the deposition at the Qingyuan site was 1.5 times the multiannual wet deposition fluxes from 27 sites across Europe in 2000–2017 (4.0 – $9.8 \text{ kg N ha}^{-1} \text{ year}^{-1}$) [24], higher than that at eight Japanese sites (3.0 – $12.9 \text{ kg N ha}^{-1} \text{ year}^{-1}$) [54], seven times higher than that in Mondy ($0.4 \text{ kg N ha}^{-1} \text{ year}^{-1}$), and higher than that in Ochiishi ($2 \text{ kg N ha}^{-1} \text{ year}^{-1}$) by 35 times. Thus, the N deposition level in the Qingyuan site is moderate to high. Furthermore, since our sampling gauges are open all the time, we collected all wet deposition plus part of the dry deposition, i.e., bulk deposition. Dry deposition can account for half to two-thirds of the total nitrogen deposition in many cases [5,55]. Thus, our measured bulk deposition could be lower than the total N deposition at the study forest (wet + dry deposition). Dry deposition fluxes (1.1 to $52.2 \text{ kg N ha}^{-1} \text{ year}^{-1}$) of Nr species on average contributed 52% to the total N deposition (2.9 to $83.3 \text{ kg N ha}^{-1} \text{ year}^{-1}$) across the 43 monitoring sites in China, indicating the importance of dry deposition monitoring for a complete N deposition assessment at the national scale. Future studies are needed to measure both wet and dry deposition separately to better depict the impacts of N deposition forest ecosystems in northeastern China.

4.2. Seasonal Variations, Sources, and Controlling Factors of Ion Concentration & Deposition

The NO_3^- , SO_4^{2-} , NH_4^+ , and Mg^{2+} concentrations at the Qingyuan site showed significant seasonal variation (Figure 3, Table 2). The NH_4^+ concentrations in precipitation were slightly higher in winter than in spring and summer, significantly higher than in autumn, and approximately 2.6 times higher than in autumn ($p < 0.05$, Table 2). The high concentrations in winter are may results from the increase in the combustion of fossil fuels (coal-based) and biomass fuels (straw- and fuelwood-based) [56], an increase in motor vehicle emissions [57,58], and the low temperature and precipitation in winter and stable meteorological conditions that slow the diffusion and dilution of NH_3 . The higher NH_4^+ concentrations in spring and summer may be due to increased NH_3 volatilisation from

livestock manure decomposition and fertiliser application caused by high temperatures, being consistent with findings reported by Chang et al. (2016), Gu et al. (2015), and David et al. (2014) [58–60]. In addition, higher precipitation in autumn and the dilution effect of precipitation on NH_3 and NH_4^+ in the atmosphere are the reasons for the low NH_4^+ concentration in precipitation in autumn.

Main sources of atmospheric NO_x include lightning, coal and biomass combustion, motor vehicle exhaust emissions, and soil biological processes (nitrification and denitrification) [61–63]. The concentrations of NO_3^- in atmospheric precipitation at our study site in winter and spring were 1.6–2.0 times higher than in summer and autumn ($p < 0.05$, Table 2), consistent with reported values in Beijing and Chizhou by Xu et al. (2015) [63]. The higher NO_3^- concentrations in winter and spring were likely due to coal and biomass combustion and NO_y (NO_x plus HNO_3 plus NO_3^-) emissions from motor vehicle exhaust [64]. Wen et al. (2020) reported that the cumulative NO_x emissions from biomass combustion were 1.7×10^4 Gg [31]. According to the Ministry of Ecology and Environment of China, in 2020, NO_y emissions from motor vehicles accounted for 40% of total pollutant emissions nationwide. In addition, the variation in NO_3^- concentration depended strongly on temperature ($r = -0.39$, $p < 0.01$, Figure S5). Despite its lower temperature, winter favours the presence of NO_3^- in the particulate matter. High temperatures and precipitation in summer and autumn are not favourable for NO_3^- to exist as particulate matter. Therefore, NO_3^- concentrations are lowest in summer and autumn [65].

There was no significant seasonal variation in NH_4^+ -N and NO_3^- -N deposition at the Qingyuan site ($p > 0.05$); however, TIN deposition was significantly greater in spring and summer than in winter (data not shown). The TIN deposition was 5.7 times higher in spring and summer (1.7 and 2.0 kg N ha⁻¹ year⁻¹, respectively) than in winter (0.4 kg N ha⁻¹ year⁻¹). Precipitation was also 4.3 and 5.0 times higher in spring and summer (49 and 105 mm, respectively) than in winter (26 mm). Therefore, we suggest that increased precipitation was one of the main reasons for the higher TIN deposition in spring and summer, similar to that observed by Fang et al. (2013) in Chengyang District, Qingdao City [30].

Emissions from agricultural sources mainly influence TIN deposition during spring and summer when agricultural activities are intensified. Fertiliser application and volatilisation of livestock manure in spring and soil biological processes (nitrification and denitrification) lead to increased atmospheric NH_x and NO_x emissions. Gu et al. (2015) obtained results similar to our site [59]. Lower winter temperatures and no fertilisation activities influence TIN deposition by coal, biomass burning, and motor vehicle exhaust emissions [61,62]. It is anticipated that N deposition might increase further with the development of the surrounding society and the acceleration of urbanization. However, the current level of N deposition in the Qingyuan forest ecosystems was found to be less serious than projected from urban/suburban data. The control of energy consumption should be strengthened in future to prevent an increase in N deposition in Chinese forest ecosystems.

There was a significant positive correlation between SO_4^{2-} and NO_3^- concentrations in precipitation at the Qingyuan site during the study period ($r = 0.72$, $p < 0.01$; Figure S5). Both anions showed similar seasonal variations as those reported by Yu et al. (2019) [65] and Zhang et al. (2021) [66]. The SO_4^{2-} concentration in the precipitation was 2–3 times higher in spring and winter than in summer and autumn ($p < 0.05$, Table 2). Sulphate⁻ in precipitation originates mainly from particulate matter emitted from coal combustion, motor vehicle exhaust, and the gas–liquid phase transformation of atmospheric SO_2 [67]. Coal-fired SO_2 emissions currently account for more than 90% of the total SO_2 emissions in China [68]. We also attribute the rise in SO_4^{2-} concentrations in precipitation in early spring and winter in northeastern China to increased coal combustion. In addition, emissions from motor vehicles contribute more than other sources in winter [21,58], resulting in SO_2 and NO_x forming heavier soot and traffic compound pollution. The SO_4^{2-} concentration in precipitation in summer and autumn was lower owing to the decrease in coal combustion. Temperature was also a factor affecting the atmospheric SO_4^{2-} concentration ($r = -0.25$, $p < 0.01$, Figure S5). High temperatures and strong oxidising substances, such as O_3 , H_2O_2 ,

and $\cdot\text{OH}$, favour the production of SO_4^{2-} in summer and autumn [68]. However, the amount of coal burned in summer and autumn is much smaller than in winter, resulting in lower atmospheric SO_2 levels. Since 71% of the total annual precipitation occurred during summer and autumn, the higher the precipitation, the more significant the SO_2 and sulphate removal, leading to a high SO_4^{2-} concentration in precipitation in summer and autumn [68].

Sulphate deposition in precipitation was significantly greater in spring than in winter, with no significant seasonal differences between summer and autumn ($p < 0.05$, Table 2). Sulphate deposition was significantly and positively correlated with precipitation and SO_4^{2-} concentration ($R = 0.43$, $p < 0.05$; Figure 4a,c), indicating that SO_4^{2-} -S deposition was seasonally synchronised with SO_4^{2-} concentration and precipitation. Although the SO_4^{2-} concentrations in precipitation were similar in winter and spring, the higher temperatures and more significant precipitation in spring than in winter were more favourable for SO_4^{2-} production. Therefore, SO_4^{2-} -S deposition in spring was significantly larger than in winter.

Calcium and Mg are characteristic elements of soil, cement, and lime. Calcium and Mg^{2+} mainly originate from construction, road dust, soil, and atmospheric entry through rainfall. The seasonal variation in Ca^{2+} concentration in precipitation at the Qingyuan site was not significant. Magnesium concentrations were greater in spring and winter (dry season) than in summer and autumn ($p < 0.05$, Table 2) because of low precipitation in spring, increased dust from soil tillage [63], and high wind carrying sand containing many minerals, including Ca^{2+} and Mg^{2+} [69]. In contrast, atmospheric Ca^{2+} and Mg^{2+} are more likely to be diluted and washed away by heavy rainfall in summer and autumn. Calcium and Mg^{2+} deposition were significantly higher in spring than in winter, approximately nineteen times and seven times as much as in winter, respectively ($p < 0.05$, Table 2). This is mainly because of the long-range transport of farmland cultivation and dust in spring and the easy freezing of the ground surface or snow and ice covering in winter, reducing the dust and long-range transport.

5. Conclusions

The present study analysed the chemical composition of precipitation and quantified the major ion deposition to a typical temperate forest in northeastern China from 2018 to 2020. With the social development and industrial structure changes in and around the Qingyuan site, the ions in the precipitation at our study site are becoming more complex, with a 72% contribution from anthropogenic sources. The total inorganic N (TIN) deposition in precipitation ranged from 12.3 to 15.9 $\text{kg N ha}^{-1} \text{ year}^{-1}$, accounting for 24–44% of the total annual ion deposition (44 $\text{kg N ha}^{-1} \text{ year}^{-1}$). This indicates that N deposition in forest ecosystems in northeastern China is currently at a medium to high level. To mitigate the increase in N deposition, joint prevention and control of air pollution at the Qingyuan station and the surrounding areas should be strengthened. Agricultural sources (fertiliser application and livestock manure), non-agricultural sources (motor vehicle emissions, fossil fuel combustion, and biomass burning), and the transport of distant water vapour clouds led to seasonal variations in ion concentration and deposition at the study site. This study only analysed the three primary sources of atmospheric precipitation ions. We suggest future studies to use the stable isotope natural abundance technique to analyse more specific sources of ions in the precipitation in the study region.

Supplementary Materials: The following supporting information can be downloaded at <https://www.mdpi.com/article/10.3390/f13122024/s1>: Figure S1: Bulk deposition samplers in Qingyuan rural sites; Figure S2: The correlation between total anion and cation concentrations in precipitation in the Qingyuan forests over the study period from 2018 to 2020; Figure S3: Contribution of each source to total ions in precipitation in the Qingyuan forest over the study period, compared to Beijing, Mondy, and Ochiishi.; Figure S4: 500 m above ground level air mass backward trajectory analysis for the year 2020 from the NOAA HYSPLIT model. The blue circle indicates our study site (the Qingyuan station). The red star indicates Beijing. The grey lines represent the 72 h backward trajectories of all air masses in each season (spring, summer, autumn, winter) that end in a trajectory at this study site.

Spring from March to May, summer from June to August, autumn from September to November and winter from December to February. The red, blue, and green lines show the sources of water vapour in different directions; Figure S5: Correlation of concentrations of major ions in precipitation at the Qingyuan station: blue indicates a positive correlation, red indicates a negative correlation, and the number is the correlation coefficient in the ellipse. ** indicates a significant correlation at the 0.05 level (two-sided), *** indicates a significant correlation at the 0.01 level (two-sided). Table S1: To calculate the different sources of ions in Qingyuan precipitation, the reference values for the ratio of $[X/Na^+]_{seawater}$ and $[X/Ca^{2+}]_{soil}$ in Equations (3) to (5) were used to calculate the relative contributions of the sea salt fraction (SSF), crust fraction (CF), and anthropogenic source fraction (AF).

Author Contributions: Conceptualisation, Y.W. and Y.F.; methodology, Y.W. and Y.F.; software, Y.W.; validation, Y.W. and Y.F. formal analysis, Y.W.; investigation, X.F., D.H., and K.H.; data curation, Y.W.; writing—original draft preparation, Y.W.; writing—review and editing, Y.W., Y.F., F.Z., R.K., L.S., S.H., A.S.M. and G.A.G.; visualisation, Y.W. and Y.F.; supervision, Y.F.; funding acquisition, Y.F. and F.Z. All authors have read and agreed to the published version of the manuscript.

Funding: This research was funded by the Strategic Priority Research Program of the Chinese Academy of Sciences (grant number XDA28020302, XDA23070103), the Liaoning Vitalization Talents Program (XLYC1902016), the National Natural Science Foundation of China (31770498, 32101291, 31901134), and the Science and Technology Program of Shenyang (No. 21-108-9-06, 22-315-6-18).

Data Availability Statement: The data are included in the article.

Acknowledgments: We greatly thank Jin Li, Jianfei Wang, Dong Liu, Deze Liu, and Nanxue Liu for their assistance in laboratory work, as well as Yue Liu for R-code suggestions. We are grateful to Qingyuan Forest CERN, the Chinese Academy of Sciences for providing the experimental sites and relevant support.

Conflicts of Interest: The authors declare no conflict of interest.

References

- Galloway, J.N.; Dentener, F.J.; Capone, D.G.; Boyer, J.N.; Howarth, R.W.; Seitzinger, S.P.; Asner, G.P.; Cleveland, C.C.; Green, P.A.; Holland, E.A.; et al. Nitrogen Cycles: Past, Present, and Future. *Biogeochemistry* **2004**, *70*, 153–226. [[CrossRef](#)]
- Neff, J.C.; Ballantyne, A.P.; Farmer, G.L.; Mahowald, N.M.; Conroy, J.L.; Landry, C.C.; Overpeck, J.T.; Painter, T.H.; Lawrence, C.R.; Reynolds, R.L. Increasing eolian dust deposition in the western United States linked to human activity. *Nat. Geosci.* **2008**, *1*, 189–195. [[CrossRef](#)]
- Fowler, D.; Coyle, M.; Skiba, U.; Sutton, M.A.; Cape, J.N.; Stefan, R.; Sheppard, L.J.; Jenkins, A.; Grizzetti, B.; Galloway, J.N.; et al. The global nitrogen cycle in the twenty-first century. *Philos. Trans. R. Soc. Biol. Sci.* **2013**, *368*, 20130164. [[CrossRef](#)]
- Geng, L.; Alexander, B.; Cole-Dai, J.; Steig, E.J.; Savarino, J.; Sofen, E.D.; Schauer, A.J. Nitrogen isotopes in ice core nitrate linked to anthropogenic atmospheric acidity change. *Proc. Natl. Acad. Sci. USA* **2014**, *111*, 5808–5812. [[CrossRef](#)]
- Vet, R.; Artz, R.S.; Carou, S.; Shaw, M.; Ro, C.U.; Aas, W.; Baker, A.; Bowersox, V.C.; Dentener, F.; Galy-Lacaux, C.; et al. A global assessment of precipitation chemistry and deposition of sulfur, nitrogen, sea salt, base cations, organic acids, acidity and pH, and phosphorus. *Atmos. Environ.* **2014**, *93*, 3–100. [[CrossRef](#)]
- Rao, P.S.P.; Tiwari, S.; Matwale, J.L.; Pervez, S.; Tunved, P.; Safai, P.D.; Steig, E.J.; Savarino, J.; Sofen, E.D.; Schauer, A.J. Sources of chemical species in rainwater during monsoon and non-monsoonal periods over two mega cities in India and dominant source region of secondary aerosols. *Atmos. Environ.* **2016**, *146*, 90–99. [[CrossRef](#)]
- Deboudt, K.; Flament, P.; Bertho, M.L. Cd, Cu, Pb and Zn Concentrations in Atmospheric Wet Deposition at a Coastal Station in Western Europe. *Water Air Soil Pollut.* **2004**, *151*, 335–359. [[CrossRef](#)]
- Wang, B.; Harder, T.; Kelly, S.; Piens, D.S.; China, S.; Kovarik, L.; Keiluweit, M.; Arey, B.W.; Gilles, M.K.; Alexander, L. Airborne soil organic particles generated by precipitation. *Nat. Geosci.* **2016**, *9*, 433–437. [[CrossRef](#)]
- Niu, S.; Classen, A.; Dukes, J.; Kardol, P.; Liu, L.; Luo, Y.; Rustad, L.; Sun, J.; Tang, J.; Templer, P.; et al. Global patterns and substrate-based mechanisms of the terrestrial nitrogen cycle. *Ecol. Lett.* **2016**, *19*, 697–709. [[CrossRef](#)]
- Liu, M.; Huang, X.; Song, Y.; Tang, J.; Cao, J.; Zhang, X.; Zhang, Q.; Wang, S.; Xu, T.; Kang, L.; et al. Ammonia emission control in China would mitigate haze pollution and nitrogen deposition but worsen acid rain. *Proc. Natl. Acad. Sci. USA* **2019**, *116*, 7760–7765. [[CrossRef](#)]
- Aber, J.; McDowell, W.; Nadelhoffer, K.; Magill, A.; Glenn, B.; Mark, K.; Steven, M.; William, C.; Lindsey, R.; Ivan, F. Nitrogen saturation in temperate forest ecosystems hypotheses revisited. *Bioscience* **1998**, *48*, 921–934. [[CrossRef](#)]
- Zhang, L.Y.; Qiao, B.Q.; Wang, H.B.; Mi, T.; Cui, J.; Fu, C.; Huang, Y.; Yan, F. Chemical Characteristics of Precipitation in a Typical Urban Site of the Hinterland in Three Gorges Reservoir, China. *J. Chem.* **2018**, 2914313. [[CrossRef](#)]
- Dai, W.; Bai, E.; Li, W.; Jing, P.; Dai, G.; Zheng, X. Predicting plant–soil N cycling and soil N₂O emissions in a Chinese old-growth temperate forest under global changes: Uncertainty and implications. *Soil Ecol. Lett.* **2020**, *2*, 73–82. [[CrossRef](#)]

14. Zhao, Y.; Zhang, L.; Chen, Y.; Liu, X.; Xu, W.; Pan, Y.; Duan, L. Atmospheric nitrogen deposition to China: A model analysis on nitrogen budget and critical load exceedance. *Atmos. Environ.* **2017**, *153*, 32–40. [[CrossRef](#)]
15. Yatkin, S.; Adali, M.; Bayram, A. A study on the precipitation in Izmir, Turkey: Chemical composition and source apportionment by receptor models. *J. Atmos. Chem.* **2016**, *73*, 241–259. [[CrossRef](#)]
16. Duan, L.; Yu, Q.; Zhang, Q.; Wang, Z.; Pan, Y.; Larssen, T.; Jie, T.; Jan, M. Acid deposition in Asia: Emissions, deposition, and ecosystem effects. *Atmos. Environ.* **2016**, *146*, 55–69. [[CrossRef](#)]
17. Kuribayashi, M.; Ohara, T.; Morino, Y.; Uno, I.; Kurokawa, J.; Hara, H. Long-term trends of sulfur deposition in East Asia during 1981–2005. *Atmos. Environ.* **2012**, *59*, 461–475. [[CrossRef](#)]
18. Jia, Y.; Yu, G.; He, N.; Zhan, X.; Fang, H.; Sheng, W.; Zuo, Y.; Zhang, D.; Wang, Q. Spatial and decadal variations in inorganic nitrogen wet deposition in China induced by human activity. *Sci. Rep.* **2014**, *4*, 3763. [[CrossRef](#)] [[PubMed](#)]
19. Liu, X.; Zhang, Y.; Han, W.; Tang, A.; Shen, J.; Cui, Z.; Vitousek, P.; Jan, W.E.; Keith, G.; Peter, C.; et al. Enhanced nitrogen deposition over China. *Nature* **2013**, *494*, 459–462. [[CrossRef](#)]
20. Zhao, Y.; Xi, M.; Zhang, Q.; Dong, Z.; Ma, M.; Zhou, K.; Xu, W.; Xing, J.; Zheng, B.; Zhang, W.; et al. Decline in bulk deposition of air pollutants in China lags behind reductions in emissions. *Nat. Geosci.* **2022**, *15*, 190–195. [[CrossRef](#)]
21. Pan, Y.P.; Wang, Y.S.; Tang, G.Q.; Wu, D. Wet and dry deposition of atmospheric nitrogen at ten sites in Northern China. *Atmos. Chem. Phys.* **2012**, *12*, 6515–6535. [[CrossRef](#)]
22. Endo, T.; Yagoh, H.; Sato, K.; Kazuhide, M.; Kentaro, H.; Izumi, N.; Kiyoshi, S. Regional characteristics of dry deposition of sulfur and nitrogen compounds at EANET sites in Japan from 2003 to 2008. *Atmos. Environ.* **2011**, *45*, 1259–1267. [[CrossRef](#)]
23. Zappi, L.; Popovicheva, O.; Tositti, L.; Chichava, M.; Eremina, I.; Kasper-Giebl, A.; Tsai, Y.I.; Vlasov, D.; Kasimov, N. Factors influencing aerosol and precipitation ion chemistry in urban background of Moscow megacity. *Atmos. Environ.* **2023**, *294*, 1352–2310. [[CrossRef](#)]
24. Keresztesi, Á.; Birsan, M.V.; Nita, I.A.; Bodor, Z.; Szép, R. Assessing the neutralisation, wet deposition and source contributions of the precipitation chemistry over Europe during 2000–2017. *Environ. Sci. Eur.* **2019**, *31*, 1–15. [[CrossRef](#)]
25. Engardt, M.; Simpson, D.; Schwikowski, M.; Granat, L. Deposition of sulphur and nitrogen in Europe 1900–2050. Model calculations and comparison to historical observations. *Tellus B Chem. Phys. Meteorol.* **2017**, *69*, 1. [[CrossRef](#)]
26. Schmitz, A.; Sanders, T.G.M.; Bolte, A.; Bussotti, F.; Dirnböck, T.; Johnson, J.; Peñuelas, J.; Pollastrini, M.; Prescher, A.-K.; Sardans, J.; et al. Responses of forest ecosystems in Europe to decreasing nitrogen deposition. *Environ. Pollut.* **2019**, *244*, 980–994. [[CrossRef](#)]
27. Mindas, J.; Hanzelova, M.; Skvareninova, J.; Skvarenina, J.; Dursky, J.; Tothova, S. Long-Term Temporal Changes of Precipitation Quality in Slovak Mountain Forests. *Water* **2020**, *12*, 2920. [[CrossRef](#)]
28. Liu, X.; Xiao, H.; Xiao, H.; Song, W.; Sun, X.; Zheng, X.; Liu, Q.; Koba, K. Stable isotope analyses of precipitation nitrogen sources in Guiyang, southwestern China. *Environ. Pollut.* **2017**, *230*, 486–494. [[CrossRef](#)]
29. Fang, Y.T.; Koba, K.; Wang, X.M.; Wen, D.Z.; Li, J.; Takebayashi, Y.; Liu, X.Y.; Yoh, M. Anthropogenic imprints on nitrogen and oxygen isotopic composition of precipitation nitrate in a nitrogen-polluted city in southern China. *Atmos. Chem. Phys.* **2011**, *11*, 1313–1325. [[CrossRef](#)]
30. Fang, Y.T.; Wang, X.M.; Zhu, F.F.; Wu, Z.Y.; Li, J.; Zhong, L.; Chen, D.; Yoh, M. Three-decade changes in chemical composition of precipitation in Guangzhou city, southern China: Has precipitation recovered from acidification following sulphur dioxide emission control? *Tellus B Chem. Phys. Meteorol.* **2013**, *65*, 1. [[CrossRef](#)]
31. Wen, X.; Zhang, W.; Shang, B.; Dore, A.J.; Tang, A.; Xia, X.; Zheng, A.; Han, M.; Zhang, L.; Zhao, Y.; et al. Precipitation chemistry and atmospheric nitrogen deposition at a rural site in Beijing, China. *Atmos. Environ.* **2020**, *223*, 1352–2310. [[CrossRef](#)]
32. Sun, S.; Liu, S.; Li, L.J.; Zhao, W.J. Components, acidification characteristics, and sources of atmospheric precipitation in Beijing from 1997 to 2020. *Atmos. Environ.* **2021**, *266*, 1352–2310. [[CrossRef](#)]
33. Takahashi, M.; Feng, Z.; Mikhailova, T.A.; Kalugina, O.V.; Shergina, O.V.; Afanasieva, L.V.; Heng, R.K.J.; Majid, N.M.A.; Sase, H. Air pollution monitoring and tree and forest decline in East Asia: A review. *Sci. Total Environ.* **2020**, *742*, 140288. [[CrossRef](#)] [[PubMed](#)]
34. Aunan, K.; Hansen, M.H.; Liu, Z.; Wang, S. The Hidden Hazard of Household Air Pollution in Rural China. *Environ. Sci. Policy* **2019**, *93*, 1462–9011. [[CrossRef](#)]
35. Xu, W.; Luo, X.S.; Pan, Y.P.; Zhang, L.; Tang, A.H.; Shen, J.L.; Zhang, Y.; Li, K.H.; Wu, Q.H.; Yang, D.W.; et al. Quantifying atmospheric nitrogen deposition through a nationwide monitoring network across China. *Atmos. Chem. Phys.* **2015**, *15*, 12345–12360. [[CrossRef](#)]
36. Zhu, J.J.; Mao, Z.H.; Hu, L.; Zhang, J. Plant diversity of secondary forests in response to anthropogenic disturbance levels in montane regions of northeastern China. *J. For. Res.* **2007**, *12*, 403–416. [[CrossRef](#)]
37. Huang, S.N.; Wang, F.; Elliott, E.M.; Zhu, F.F.; Zhu, W.; Koba, K.; Yu, Z.; Hobbie, E.A.; Michalski, G.; Kang, R.; et al. Multiyear Measurements on $\Delta^{17}\text{O}$ of Stream Nitrate Indicate High Nitrate Production in a Temperate Forest. *Environ. Sci. Technol.* **2020**, *54*, 4231–4239. [[CrossRef](#)]
38. Huang, S.N.; Emily, M.; Elliott, J.; Felix, D.; Pan, Y.; Liu, D.; Li, S.; Li, Z.; Zhu, F.; Zhang, N.; et al. Seasonal pattern of ammonium ^{15}N natural abundance in precipitation at a rural forested site and implications for NH_3 source partitioning. *Environ. Pollut.* **2019**, *247*, 541–549. [[CrossRef](#)]
39. Li, Z.J.; Li, Z.X.; Song, L.L.; Gui, J.; Xue, J.; Zhang, B.L.; Gao, W.D. Precipitation chemistry in the source region of the yangtze river. *Atmos. Res* **2020**, *245*, 105073. [[CrossRef](#)]

40. Ayer, G.P. Some Practical Aspects of Acid Deposition Measurements. In Proceedings of the 3rd Expert Meeting on Acid Deposition Monitoring Network in East Asia, Niigata, Japan, 14–16 November 1995.
41. EANET. *Technical Manual for Wet Deposition Monitoring in East Asia-2010*; Asia Center for Air Pollution Research: Niigata, Japan, 2010; 113p.
42. Li, L.; Li, H.; Peng, L.; Li, Y.S.; Zhou, Y.; Chai, F.H.; Mo, Z.; Chen, Z.; Ma, J.; Wang, W. Characterization of precipitation in the background of atmospheric pollutants reduction in Guilin: Temporal variation and source apportionment. *J. Environ. Sci.* **2020**, *98*, 1–13. [[CrossRef](#)]
43. Keene, W.C.; Pszenny, A.A.; Galloway, J.N.; Hawley, M.E. Sea-salt corrections and interpretation of constituent ratios in marine precipitation. *Geophys. Res.-Atmos.* **1986**, *91*, 6647–6658. [[CrossRef](#)]
44. Taylor, S.R. Abundance of chemical elements in the continental crust: A new table. *Geochim. Cosmochim. Acta* **1964**, *28*, 1273–1285. [[CrossRef](#)]
45. Kristina, E.; Kim, H.; Torunn, B.; Norbert, S.; Sverre, S. Springtime depletion of tropospheric ozone, gaseous elemental mercury and non-methane hydrocarbons in the European Arctic, and its relation to atmospheric transport. *Atmos. Environ.* **2007**, *41*, 8511–8526. [[CrossRef](#)]
46. Barras, V.J.I.; Simmonds, I. Synoptic controls upon $d^{18}O$ in southern Tasmanian episodic events. *Geophys. Res.* **2008**, *102*, 2681–2687. [[CrossRef](#)]
47. Draxler, R.R.; Rolph, G.D. *HYSPLIT (HYbrid Single-Particle Lagrangian Integrated Trajectory) Model Access via NOAA ARL READY Website*; NOAA Air Resources Laboratory: Silver Spring, MD, USA, 2010.
48. Hemraj, B.; Lekhendra, T.; Shichang, K.; Chhatra, M.S.; Pengfei, C.; Junming, G.; Prakriti, S.G. Concentration sources and wet deposition of dissolved nitrogen and organic carbon in the Northern Indo-Gangetic Plain during monsoon. *J. Environ. Sci.* **2021**, *102*, 37–52. [[CrossRef](#)]
49. Tripathee, L.; Kang, S.; Huang, J.; Sillanpaa, M.; Sharma, C.M.; Lüthi, Z.L.; Guo, J.; Paudyal, R. Ionic composition of wet precipitation over the southern slope of Central Himalayas. *Nepal. Environ. Sci. Pollut. Res.* **2014**, *21*, 2677–2687. [[CrossRef](#)]
50. Khan, M.F.; Nizam, K.; Maulud, A.K.N.; Latif, M.T.; Jing, X.; Norhaniza, A.; Azwani, A.; Mohd, S.M.N.; Mazrura, S.; Maznorizan, M.; et al. Physicochemical factors and their potential sources inferred from long-term rainfall measurements at an urban and a remote rural site in tropical areas. *Sci. Total Environ.* **2018**, *613–614*, 1401–1416. [[CrossRef](#)]
51. Adhikari, S.; Zhang, F.; Adhikari, N.P.; Zeng, C.; Pant, R.R.; Ram, K.; Liu, Y.; Ahmed, N.; Xu, J.; Tripathee, L.; et al. Atmospheric wet deposition of major ionic constituents and inorganic nitrogen in Bangladesh: Implications for spatiotemporal variation and source apportionment. *Atmos. Res.* **2021**, *250*, 0169–8095. [[CrossRef](#)]
52. Meng, Y.; Zhao, Y.; Li, R.; Li, J.; Cui, L.; Kong, L.; Fu, H. Characterization of inorganic ions in rainwater in the megacity of Shanghai: Spatiotemporal variations and source apportionment. *Atmos. Res.* **2019**, *222*, 12–24. [[CrossRef](#)]
53. Wen, Z.; Xu, W.; Li, Q.; Han, M.; Tang, A.; Zhang, Y.; Luo, X.; Shen, J.; Wang, W.; Li, K.; et al. Changes of nitrogen deposition in China from 1980 to 2018. *Environ. Int.* **2020**, *144*, 106022. [[CrossRef](#)]
54. Ban, S.; Matsuda, K.; Sato, K.; Ohizumi, T. Long-term assessment of nitrogen deposition at remote EANET sites in Japan. *Atmos. Environ.* **2016**, *146*, 70–78. [[CrossRef](#)]
55. Li, Q.; Jiang, J.; Cai, S.; Zhou, W.; Wang, S.; Duan, L.; Hao, J. Gaseous Ammonia Emissions from Coal and Biomass Combustion in Household Stoves with Different Combustion Efficiencies. *Environ. Sci. Technol. Lett.* **2016**, *3*, 98–103. [[CrossRef](#)]
56. Farren, N.J.; Davison, J.; Rose, R.A.; Wagner, R.L.; Carslaw, D.C. Underestimated Ammonia Emissions from Road Vehicles. *Environ. Sci. Technol.* **2020**, *54*, 15689–15697. [[CrossRef](#)] [[PubMed](#)]
57. Song, L.; Walters, W.W.; Pan, Y.; Li, Z.; Gu, M.; Duan, Y.; Lü, X.; Fang, Y. ^{15}N natural abundance of vehicular exhaust ammonia, quantified by active sampling techniques. *Atmos. Environ.* **2021**, *255*, 118430. [[CrossRef](#)]
58. Chang, Y.; Zou, Z.; Deng, C.; Kan, H.; Collett, J.L.; Lin, J.; Zhuang, G. The importance of vehicle emissions as a source of atmospheric ammonia in the megacity of Shanghai. *Atmos. Chem. Phys.* **2016**, *16*, 3577–3594. [[CrossRef](#)]
59. Gu, B.; Ju, X.; Chang, J.; Ge, Y.; Vitousek, P.M. Integrated reactive nitrogen budgets and future trends in China. *Proc. Natl. Acad. Sci. USA* **2015**, *112*, 8792–8797. [[CrossRef](#)]
60. Felix, J.D.; Elliott, E.M.; Gish, T.; Ronaldo, M.; Leah, C.; Jane, C. Examining the transport of ammonia emissions across landscapes using nitrogen isotope ratios. *Atmos. Environ.* **2014**, *95*, 563–570. [[CrossRef](#)]
61. Shi, Y.; Xia, Y.; Lu, B.; Liu, N.; Zhang, L.; Li, S.; Li, W. Emission inventory and trends of NO_x for China, 2000–2020. *J. Zhejiang Univ. Sci. A* **2014**, *15*, 454–464. [[CrossRef](#)]
62. Fang, Y.T.; Koba, K.; Makabe, A.; Chieko, T.; Zhu, W.; Hayashi, T.; Hokari, A.A.; Urakawa, R.; Bai, E.; Houlton, B.Z.; et al. Microbial denitrification dominates nitrate losses from forest ecosystems. *Proc. Natl. Acad. Sci. USA* **2015**, *112*, 1470–1474. [[CrossRef](#)]
63. Xu, Z.F.; Wu, Y.L.; Liang, W.J.; Ji, C.S.; Ji, J.; Zhao, T.; Zhang, X. Chemical composition of rainwater and the acid neutralizing effect at Beijing and Chizhou city, China. *Atmos. Res.* **2015**, *164–165*, 278–285. [[CrossRef](#)]
64. Tao, J.; Zhang, L.M.; Engling, G.; Zhang, R.; Yang, Y.; Cao, J.; Zhu, C.; Wang, Q.; Luo, L. Chemical JEE composition of PM_{2.5} in an urban environment in Chengdu, China: Importance of springtime dust storms and biomass burning. *Atmos. Res.* **2013**, *122*, 270–283. [[CrossRef](#)]
65. Yu, G.; Jia, Y.; He, N.; Zhu, J.; Chen, Z.; Wang, Q.; Piao, S.; Liu, X.; He, H.; Guo, X.; et al. Stabilization of atmospheric nitrogen deposition in China over the past decade. *Nat. Geosci.* **2019**, *12*, 424–429. [[CrossRef](#)]

66. Zhang, Z.; Guan, H.; Xiao, H.; Yue, L.; Zheng, N.; Li, L.; Liu, C.; Fang, X.; Xiao, H. Oxidation and sources of atmospheric NO_x during winter in Beijing based on $\delta^{18}\text{O}$ - $\delta^{15}\text{N}$ space of particulate nitrate. *Environ. Pollut.* **2021**, *276*, 116708. [[CrossRef](#)]
67. Chang, C.T.; Yang, C.J.; Huang, K.H.; Huang, J.C.; Lin, T.C. Changes of precipitation acidity related to sulfur and nitrogen deposition in forests across three continents in north hemisphere over last two decades. *Sci. Total Environ.* **2022**, *806*, 0048–9697. [[CrossRef](#)] [[PubMed](#)]
68. Aas, W.; Mortier, A.; Bowersox, V.; Cherian, R.; Faluvegi, G.; Fagerli, H.; Hand, J.; Klimont, Z.; Galy-Lacaux, C.; Lehmann, C.M.B.; et al. Global and regional trends of atmospheric sulfur. *Sci Rep.* **2019**, *9*, 953. [[CrossRef](#)]
69. Wang, H.; Han, G.L. Chemical composition of rainwater and anthropogenic influences in Chengdu, Southwest China. *Atmos. Res.* **2011**, *99*, 190–196. [[CrossRef](#)]